Design of LCC Impedance Matching Circuit for Wireless Power Transfer System Under Rectifier Load

Chenglin Liao, Junfeng Li, and Shufan Li

***Abstract*—In wireless power transfer system, impedance matching circuits are usually used to match the impedance between actual load and the optimal load, to achieve the maximum transfer efficiency (coil to coil efficiency). It is easily to design impedance matching circuit parameters for linear load. However, the load is always the rectifier one in many applications. The equivalent impedance of rectifier load is complex impedance, which is affected not only by itself, but also by pre-stage circuit, such as impedance matching circuit parameters. It is hard to calculate the equivalent impedance of rectifier load directly to design the impedance matching circuit parameters. This paper investigates the LCC impedance matching design method for secondary side under rectifier load. Firstly, the transfer efficiency characteristic under rectifier load is studied, and the equivalent impedance is analyzed according to transfer efficiency. Then the impedance calculation method of secondary side under rectifier load is derived via formula derivation and Fourier series theory, and the LCC circuit parameters design method is proposed. Lastly, a wireless charging system for electric vehicle is established to verify the method that can transfer 3.3 kW power over 20 cm distance with 92.7% system efficiency (end to end efficiency).**

***Index Terms*—Impedance calculation, LCC Impedance matching, magnetic resonance coupling, optimization, rectifier load.**

I. Introduction

RECENTLY, wireless power transfer technology (WPT) is widely used in charging platforms of mobile device, biomedical implants, wireless sensor networks, electric vehicle, and many other applications [1]-[4].Compared to wired way, WPT is more safe, convenient, automated and environmentally adaptive. In 2007, a new WPT design method via magnetic resonant coupling (MRC) was proposed to enlarge the distance, improve the transmission power and efficiency, especially in middle range charging applications [5], [6].

For a common MRC system with two coils structure, primary coil and secondary coil, the circuit loop of secondary side is working at resonant condition [7], [8], and the transfer efficiency is affected by the coupling coefficient, quality factor, frequency, load and other parameters. There exists the optimum load value to achieve maximum transfer efficiency [9], [10]. However, the actual load is not always equal to the optimum value, so impedance matching circuits are used to match the impedance between actual load and optimum load [11]-[13]. There are many topologies of impedance matching circuit, and the circuit parameters can be easily designed using analytical or numerical method for linear load, such as resistive load, R-C (resistance and capacitance) load and R-L (resistance and inductance) load [14]-[17].

In many applications, such as electric vehicle wireless charger and mobile phone wireless charger, WPT system outputs are direct voltage and current, and always use rectifier circuit to convert high frequency alternating current into direct current, and then supply DC power for actual load, or other DC-DC converters [18]-[20]. Thus the load of secondary coil is a nonlinear rectifier load, and the impedance matching design becomes more complicated than linear load. The equivalent impedance of rectifier load is complex, containing resistive part and imaginary part, and the equivalent value is affected not only by its parameters, but also by the pre-stage impedance matching circuit, which cannot be easily simplified into linear impedance. So it is difficult to design the impedance matching circuit parameters for secondary side coil under rectifier load.

As mentioned in literature [21], a double-sided LCC compensation network and its tuning method was proposed for wireless EV charging system, which ensured the resonant frequency is irrelevant with the coupling coefficient between the two coils and is also independent of the load condition. But it doesn't take the nonlinear rectifier load into consideration. In literature [22], a Series/Series-Parallel topology was analyzed to achieve constant voltage output. In literature [23], the steady state track current was load independent using the LCL-T based impedance matching circuit. Despite various compensation methods, few of them were based on the nonlinear analysis of the rectifier load, instead considering the rectifier load as a resistance load.

This paper theoretically analyzes the working process of rectifier load together with LCC impedance matching circuit, and then deduces the analytical expressions of the voltage and current in circuit at each operation modes using Fourier series theory. Furthermore, the equivalent impedance calculation method of rectifier load is derived based on the fundamental component. Last but not the least, the secondary side impedance matching circuit parameters can be determined to achieve maximum transfer efficiency (coil to coil efficiency) for MRC system in an experimental way.

Manuscript received August 27, 2017. This work was supported by Beijing Municipal Science & Technology Commission under program under Grant D121100004512001.

C. Liao is with the Key Laboratory of Power Electronics and Electrical Drives, Institute of Electrical Engineering, Chinese Academy of Sciences, Beijing 100190, China (e-mail: liaocl@mail.iee.ac.cn). J. Li is with Beijing Institute of Space Launch Technology, Beijing 100076, China (e-mail: lijunfeng2006@126.com). S. Li is with University of Chinese Academy of Sciences, Beijing 100190, China (e-mail: lishufan@ mail.iee.ac.cn).

Digital Object Identifier 10.24295/CPSSTPEA.2017.00022

II. Basic Analysis of Wireless Power Transfer

A. Basic Theory Model Under Resistive Load

The simplified typical circuit of WPT system with two coils structure, as Fig. 1 shows, contains voltage source U_I, primary capacitor C_P, primary coil inductor L_P, primary coil resistor R_P, secondary capacitor C_S, secondary coil inductor L_S, secondary resistor R_S, and load R_L.M_{PS} is the mutual inductance between primary coil and secondary coil.

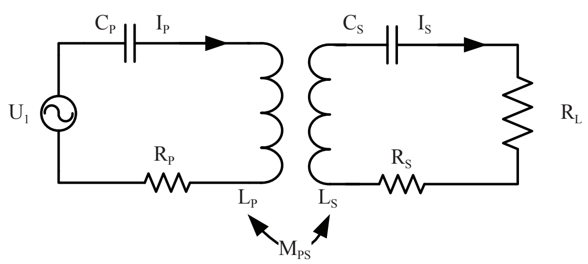

Fig. 1. Simplified typical circuit of WPT under resistance load.

The typical circuit can be described in matrix equations (1) [24]. The power loss P_t, load power P_L, and efficiency η satisfy (2)-(4), where ω is operation radian frequency.

$$\begin{bmatrix} U_I \\ 0 \end{bmatrix} = \begin{bmatrix} j\omega L_P + 1/(j\omega C_P) + R_P & j\omega M_{PS} \\ j\omega M_{PS} & j\omega L_S + 1/(j\omega C_S) + R_S + R_L \end{bmatrix} \begin{bmatrix} I_1 \\ I_2 \end{bmatrix} \quad (1)$$

$$P_t = I_P^2 R_P + I_S^2 R_S \quad (2)$$

$$P_L = I_S^2 R_L \quad (3)$$

$$\eta = 1/(1 + P_t / P_L) \quad (4)$$

Where I_P and I_S are the virtual values of the currents of primary and secondary side, respectively.
We use $y = P_t/P_L$, and calculate y in (5), where κ_{PS} is the coupling factor between coils, Q_P and Q_S is quality factor of primary and secondary coil, $Q_{P,S} = \omega L_{P,S}/R_{P,S}$.

$$y = \frac{\left| j\omega L_S + 1/(j\omega C_S) + R_S + R_L \right|^2}{\omega \kappa_{PS}^2 L_S Q_P R_L} + \frac{\omega L_S}{Q_S R_L} \quad (5)$$

So it is obviously that $\eta \propto Q_P$, Q_S, κ_{PS}, and reaches local maximum point at $j\omega L_s + 1/(j\omega C_s) = 0$.
Equation (5) can be simplified into (6) when parameters satisfy $j\omega L_s + 1/(j\omega C_s) = 0$.

$$y = \frac{(R_S + R_L)^2}{\omega \kappa_{PS}^2 L_S Q_P R_L} + \frac{\omega L_S}{Q_S R_L} \quad (6)$$

We can get the maximum efficiency η when y reaches its minimum point. The maximum condition in (7) is satisfied when R_L equals to the optimum value R_{opt}: $R_{opt} = R_S \sqrt{1 + k_{PS}^2 Q_P Q_S}$.

$$\frac{\partial y}{\partial R_L} = \frac{1}{w k_{PS}^2 L_S Q_P} - \frac{R_S^2}{w k_{PS}^2 L_S Q_P R_L^2} - \frac{w L_S}{Q_S R_L^2} = 0 \quad (7)$$

And then the maximum efficiency η_{max} can be calculated in (8)[25],

$$\eta_{max} = \Delta / (\sqrt{1+\Delta} + 1)^2 \quad (8)$$

$$\Delta = k_{PS}{}^2 Q_P Q_S \quad (9)$$

Therefore, if L_P, L_S, κ_{PS}, R_P, R_S are known, we can obtain the maximum efficiency conditions:

$$\begin{cases} C_S = 1/(\omega^2 L_s) \\ R_L = R_{opt} \end{cases} \quad (10)$$

B. Efficiency Characteristics Under Rectifier Load

In many applications, there is not always the resistive load of secondary side coil, but the rectifier load that contains rectifier diode, large capacitance C_L and resistance R_L, as Fig. 2 shows. The resistance R_L is the actual load for users, but the rectifier load is the real load for secondary side coil.

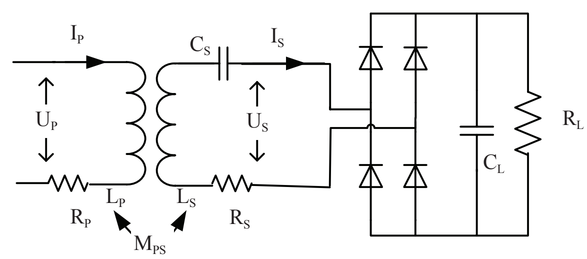

Fig. 2. Typical circuit of WPT system under rectifier load.

To study the effect of the rectifier load on the performance of the WPT system, a simulation is conducted in Matlab/Simulink test bench. The efficiency characteristic of WPT system under rectifier load is the same with system under resistance load, as Fig. 3 shows. There also exists the maximum efficiency point

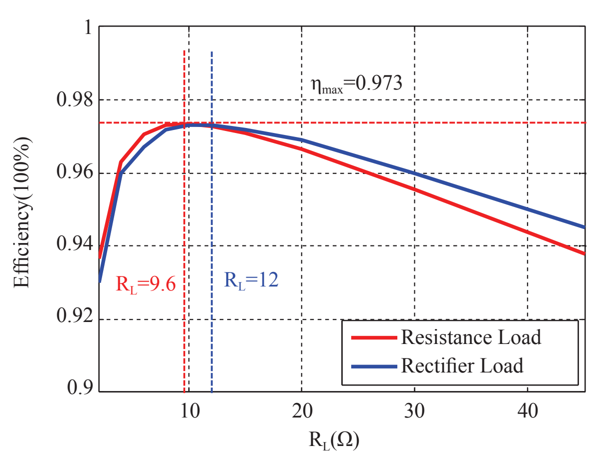

Fig. 3. Efficiency comparison between resistance load and rectifier load, where C_S = 61.1nF, C_S and L_S are working at resonant condition.

and the similar tendency, where parameters as TABLE I show.

TABLE I
WPT SYSTEM PARAMETER

Parameter	Value	Parameter	Value
L_P	164.26 uH	L_S	165.69 uH
R_P	0.101 Ω	R_S	0.129 Ω
M_{PS}	27.04 uH	*Frequency*	50 kHz
C_L	470 uF		

However, there are different efficiency characteristics between the two load types apparently. Firstly, the optimum R_L for maximum efficiency is different, as Fig. 3 shows, and larger in system under rectifier load. Secondly, at different R_L conditions, as Fig. 4 shows, the optimum capacitance C_S for WPT system under rectifier load is varying, while it is constant in system under resistance load that equals to $1/(\omega^2 L_S)$. According to Fig. 3 and Fig. 4, it can be indicated that the equivalent impedance of rectifier load is complex impedance, which contains real part and imaginary part, and the equivalent value is not only affected by its parameters, but also the pre-stage circuit parameter. When designing the impedance matching circuit between rectifier load and secondary coil, the characteristics must be taken into consideration.

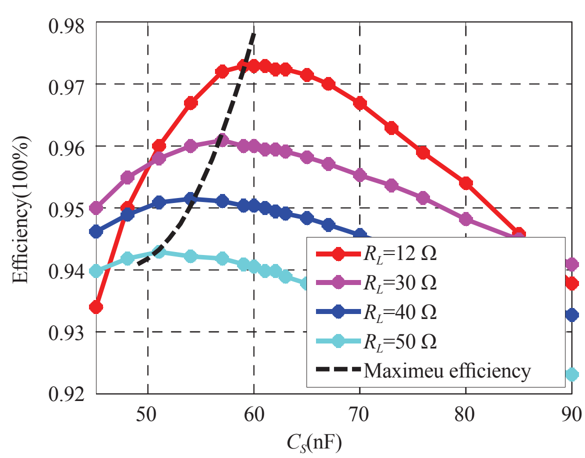

Fig. 4. Effects of C_S on efficiency at different R_L conditions of rectifier load.

III. Theory Analysis of Proposed Impedance Calculation Method for Rectifier Load Using LCC Impedance Matching Circuit

As is shown in section II, and optimum load R_{opt} should be obtained to achieve the maximum efficiency of the WPT system. However, it is obvious from Fig. 1 that the S-S impedance matching method cannot adjust the real part of the secondary side impedance, thus it cannot match the load to R_{opt} unless the real part of the rectifier load equals to R_{opt}. Taking the above analysis into consideration, the LCC impedance matching method is introduced to meet the optimum load R_{opt} for secondary coil for maximum efficiency in WPT system under rectifier load, as Fig. 5 shows, C_S, C_{21} and L_{21} forms LCC impedance matching circuit.

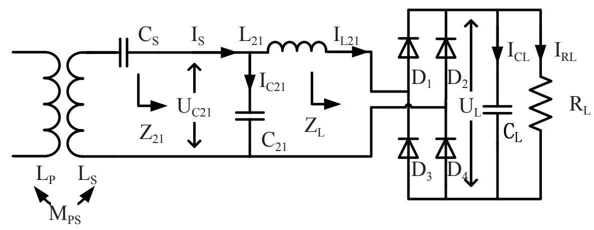

Fig. 5. LCC impedance matching circuit for rectifier load.

For conventional LCC impedance matching method, the rectifier load is seen as a resistance load. A simulation was conducted based on the data shown in TABLE I. Using the conventional LCC impedance matching method, rectifier load and resistance load were matched to the optimum load respectively, as Fig. 6 shows. It can be seen that with the conventional method, a relatively high efficiency can be achieved for resistance load, while for rectifier load, the efficiency is lower except for very small R_L. The main reason for this is that the rectifier load is seen as a resistance load in the conventional method, introducing errors which cannot be neglected. In the following part of this section, the rectifier load will be calculated to solve this problem.

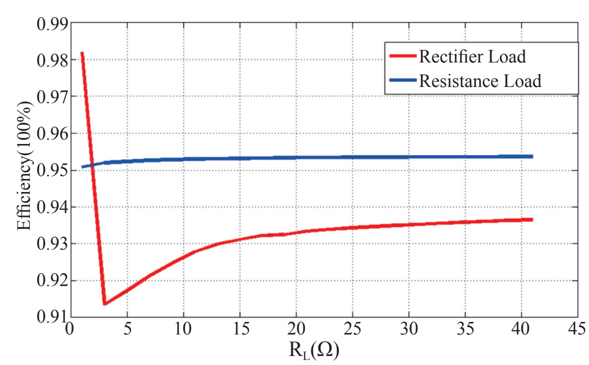

Fig. 6. Efficiency comparison between resistance load and rectifier load for conventional LCC impedance matching method.

A. Circuit Operation Analysis

Due to heavily affected by pre-stage circuit, rectifier load is combined with LCC circuit for impedance calculation. The equivalent impedance Z_{21} in Fig. 5 is analyzed to match R_{opt} via adjusting C_S, C_{21} and L_{21}.

Simulations have been conducted to study the circuit operation of the secondary side for LCC compensation method.Fig. 7 shows the operation current and voltage waveforms of secondary side circuit, of which the rectifier works in continuous conduction mode (CCM) (the working condition of the rectifier will be illustrated later). Though affected by diode nonlinear characteristic, the secondary coil current $i_S(t)$ is approximately sinusoidal waveform using LCC impedance matching circuit. We can regard i_S as a sinusoidal current source, $i_S(t)=I_S \sin(\omega t+\delta)$.

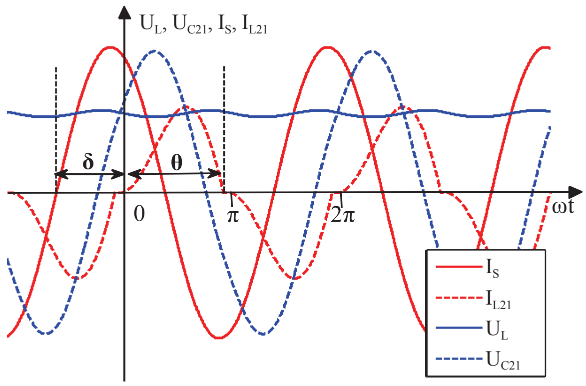

Fig. 7. Operation waveforms of LCC and Rectifier circuit (CCM state). δ is the rectifier diodes conduction lag, θ is the conduction angle of rectifier circuit.

The rectifier operation process can be described by four modes as Fig. 8 shows.

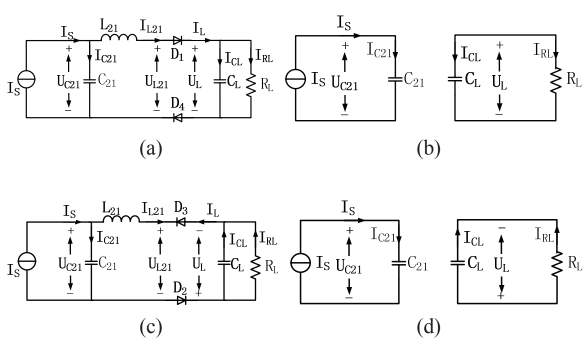

Fig. 8. Operation modes of rectifier load. (a) $0 \le \omega t < \theta$; (b) $\theta \le \omega t < \pi$; (c) $\pi \le \omega t < \pi + \theta$; (d) $\pi + \theta \le \omega t < 2\pi$.

(a) When $0 \le \omega t < \theta$:

We can establish the circuit equations as (11)-(14) according to Fig. 8(a). So $u_L(t)$ can be deduced in (15) .

$$i_{C21}(t) = C_{21}\frac{du_{C21}(t)}{dt} \tag{11}$$

$$i_{L21}(t) = \frac{u_L(t)}{R_L} + C_L\frac{du_L(t)}{dt} \tag{12}$$

$$i_{C21}(t) + i_{L21}(t) = I_S\sin(\omega t + \delta) \tag{13}$$

$$u_{C21}(t) = L_{21}\frac{di_{L21}(t)}{dt} + u_L(t) \tag{14}$$

$$\frac{d^3u_L(t)}{dt^3} + A\frac{d^2u_L(t)}{dt^2} + B\frac{du_L(t)}{dt} + Cu_L(t) = D\sin(\omega t + \delta) \tag{15}$$

Where $A = 1/(C_LR_L)$, $B = 1/(L_{21}C_{21}) + 1/(L_{21}C_L)$, $C = 1/(L_{21}C_{21}C_LR_L)$, $D = I_S/(L_{21}C_{21}C_L)$

We can obtain the characteristic equation as (16), and solve the roots $\lambda_1, \lambda_2, \lambda_3$ in (17)-(18).

$$\lambda^3 + A\lambda^2 + B\lambda + C = 0 \tag{16}$$

$$\begin{aligned}\lambda_1 = &-\left(\frac{B}{3}-\frac{A^2}{9}\right)\Big/\sqrt[3]{\sqrt{\left(\frac{A^3}{27}-\frac{AB}{6}+\frac{C}{2}\right)^2+\left(\frac{B}{3}-\frac{A^2}{9}\right)^3}-\frac{A^3}{27}+\frac{AB}{6}-\frac{C}{2}}\\ &-\frac{A}{3}+\sqrt[3]{\sqrt{\left(\frac{A^3}{27}-\frac{AB}{6}+\frac{C}{2}\right)^2+\left(\frac{B}{3}-\frac{A^2}{9}\right)^3}-\frac{A^3}{27}+\frac{AB}{6}-\frac{C}{2}}\end{aligned} \tag{17}$$

$$\begin{aligned}\lambda_{2,3} = &\left(\frac{B}{3}-\frac{A^2}{9}\right)\Big/\left[2*\sqrt[3]{\sqrt{\left(\frac{A^3}{27}-\frac{AB}{6}+\frac{C}{2}\right)^2+\left(\frac{B}{3}-\frac{A^2}{9}\right)^3}-\frac{A^3}{27}+\frac{AB}{6}-\frac{C}{2}}\right]\\ &-\frac{A}{3}-\frac{1}{2}\sqrt[3]{\sqrt{\left(\frac{A^3}{27}-\frac{AB}{6}+\frac{C}{2}\right)^2+\left(\frac{B}{3}-\frac{A^2}{9}\right)^3}-\frac{A^3}{27}+\frac{AB}{6}-\frac{C}{2}}\\ &\pm i\frac{\sqrt{3}}{2}\left[\left(\frac{B}{3}-\frac{A^2}{9}\right)\Big/\sqrt[3]{\sqrt{\left(\frac{A^3}{27}-\frac{AB}{6}+\frac{C}{2}\right)^2+\left(\frac{B}{3}-\frac{A^2}{9}\right)^3}-\frac{A^3}{27}+\frac{AB}{6}-\frac{C}{2}}\right.\\ &\left.+\sqrt[3]{\sqrt{\left(\frac{A^3}{27}-\frac{AB}{6}+\frac{C}{2}\right)^2+\left(\frac{B}{3}-\frac{A^2}{9}\right)^3}-\frac{A^3}{27}+\frac{AB}{6}-\frac{C}{2}}\right]\end{aligned} \tag{18}$$

It is obvious that λ_2, λ_3 can be described as $\lambda_{2,3} = \alpha \pm i\beta$. So the solution for homogenous equation of (15) can be described as (19), where C_1, C_2, C_3 are coefficients.

$$u_L(t) = C_1e^{\lambda_1} + e^{\alpha t}\left[C_2\cos(\beta t) + C_3\sin(\beta t)\right] \tag{19}$$

Based on further analysis, we can know that $\alpha < 0$, and $i\omega$ is not the solution of homogenous form of (15). The particular solution of (15) can be described in (20).The coefficient C_4 and C_5 are calculated by (21). Then $u_L(t)$, $i_{L21}(t)$, $u_{C21}(t)$ can be described in (22)-(24) when $0 \le \omega t < \theta$.

$$u_L^*(t) = C_4\cos(\omega t + \delta) + C_5\sin(\omega t + \delta) \tag{20}$$

$$\begin{bmatrix}\omega^3 - B\omega & C - A\omega^2\\ C - A\omega^2 & -\omega^3 + B\omega\end{bmatrix}\begin{bmatrix}C_4\\ C_5\end{bmatrix} = \begin{bmatrix}D\\ 0\end{bmatrix} \tag{21}$$

$$\begin{aligned}u_L(t) &= u_L(t) + u_L^*(t)\\ &= C_1e^{\lambda_1 t} + e^{\alpha t}\left[C_2\cos(\beta t) + C_3\sin(\beta t)\right]\\ &\quad + C_4\cos(\omega t + \delta) + C_5\sin(\omega t + \delta)\end{aligned} \tag{22}$$

$$\begin{aligned}i_{L21}(t) = &\,e^{\alpha t}(C_LC_3\beta + C_L\alpha C_2 + C_2/R_L)\cos(\beta t)\\ &+ e^{\alpha t}(C_L\alpha C_3 - C_LC_2\beta + C_3/R_L)\sin(\beta t)\\ &+ (C_LC_5\omega + C_4/R_L)\cos(\omega t + \delta)\\ &+ (C_5/R_L - C_LC_4\omega)\sin(\omega t + \delta)\\ &+ C_1e^{\lambda_1 t}(C_L\lambda_1 + 1/R_L)\end{aligned} \tag{23}$$

$$\begin{aligned}u_{C21}(t) = &\left[(\alpha^2 - \beta^2)C_LC_2 + 2\alpha\beta C_LC_3 + \frac{\alpha C_2 + \beta C_3}{R_L}\right]e^{\alpha t}\cos(\beta t)\\ &+ \left[(\alpha^2 - \beta^2)C_LC_3 - 2\alpha\beta C_LC_2 + \frac{\alpha C_3 - \beta C_2}{R_L}\right]e^{\alpha t}\sin(\beta t)\\ &- \omega(C_LC_5\omega + C_4/R_L)\sin(\omega t + \delta)\\ &+ \omega(C_5/R_L - C_LC_4\omega)\cos(\omega t + \delta)\\ &+ C_1\lambda_1e^{\lambda_1 t}(C_L\lambda_1 + 1/R_L)\end{aligned} \tag{24}$$

β in (23) reflects the high frequency component in i_{L21}(t), and satisfies (25). It is obvious that the high frequency component of diodes current is closely related to L_{21}, and the frequency β can be very high when L_{21} is very low.

$$\beta \approx \sqrt{\frac{1}{L_{21}C_{21}} + \frac{1}{L_{21}C_L} - \frac{1}{3}\left(\frac{1}{C_L R_L}\right)^2} \approx \frac{1}{\sqrt{L_{21}C_{21}}} \tag{25}$$

(b) When $\theta \le \omega t < \pi$:

At that moment, rectifier diodes turn off, and $u_L(t)$, $u_{C21}(t)$ can be described in (26)-(27).

$$u_L(t) = u_L(\theta/\omega)e^{(\theta - t)/(\omega R_L C_L)} \tag{26}$$

$$u_{C21}(t) = \frac{1}{C_{21}}\int_{\theta/\omega}^{t} i_S(t)dt + u_{C21}\left(\frac{\theta}{\omega}\right) \tag{27}$$

(c) When $\pi \le \omega t < \pi + \theta$:

According to the cycle property, we can substitute t-π/ω for t in (24) to get the expression of $-u_{C21}(t)$ when $\pi \le \omega t < \pi + \theta$.

(d) When $\pi + \theta \le \omega t < 2\pi$:

We can also substitute t-π/ω for t in (27) to get the expression of $-u_{C21}(t)$ when $\pi + \theta \le \omega t < 2\pi$.

B. Calculation of Equivalent Impedance Z_{21}

According to circuit theory, expressions of $u_L(t)$, $i_{L21}(t)$, $u_{C21}(t)$ should satisfy initial conditions in (28)-(32), so we can solve C_1, C_2, C_3, δ.

$$i_{L21}(0) = 0 \tag{28}$$

$$i_{L21}\left(\frac{\theta}{\omega}\right) = 0 \tag{29}$$

$$u_L(0) = u_L\left(\frac{\pi}{\omega}\right) \tag{30}$$

$$u_{C21}(0) = u_L(0) \tag{31}$$

$$u_{C21}\left(\frac{\pi}{\omega}\right) = -u_L\left(\frac{\pi}{\omega}\right) \tag{32}$$

Therefore, the expressions of $u_L(t)$, $i_{L21}(t)$, $u_{C21}(t)$ is determined. We use Fourier series theory to deduce the expression of $u_{C21}(t)$ in whole cycle in (33).

$$u_{C21}(t) = \frac{a_0}{2} + \sum_{n=1}^{\infty}\left[\sqrt{a_n^2 + b_n^2}\sin(n\omega t + \varphi_n)\right] \text{(n=1,2...)} \tag{33}$$

$$a_n = \frac{\omega}{\pi}\int_{-\pi/\omega}^{\pi/\omega} u_{C21}(t)\cos(nt)dt \tag{34}$$

$$b_n = \frac{\omega}{\pi}\int_{-\pi/\omega}^{\pi/\omega} u_{C21}(t)\sin(nt)dt \tag{35}$$

$$\varphi_n = \arccos\frac{b_n}{\sqrt{a_n^2 + b_n^2}} \tag{36}$$

In WPT system with optimal LCC impedance matching circuit, $u_{C21}(t)$ is approximately like sinusoidal waveforms, and containing few harmonic distortion. We can use fundamental component to calculate the equivalent impedance of Z_{21} in Fig. 5 by (37).

$$Z_{21} = \frac{U_{C21}}{I_S} = \frac{\sqrt{a_1^2 + b_1^2}}{I_S}e^{j(\varphi_1 - \delta)} \tag{37}$$

$Z_{21} = R_{21} + jX_{21}$, where R_{21} and X_{21} are the real and imaginary part of Z_{21} respectively.

Then the equivalent impedance of rectifier load Z_L is computed in (38)

$$Z_L = \frac{Z_{21}}{1 - i\omega C_{21}Z_{21}} - i\omega L_{21} \tag{38}$$

C. Special Operation Mode of LCC

When θ increases to π, the four rectifier operation modes translate into two modes as Fig. 9 shows. And we can also deduce the expression of $u_{C21}(t)$ and Z_{21} using the same method.

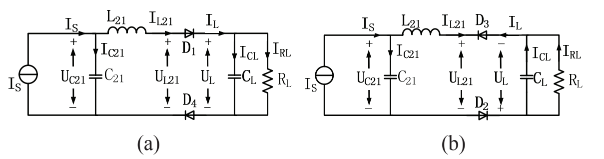

Fig. 9. Operation modes of rectifier load when $\theta = \pi$. (a) $0 \le \omega t < \pi$; (b) $\pi \le \omega t < 2\pi$.

D. Analysis of Rectifier Load Equivalent Impedance Z_R

Equivalent impedance Z_L of rectifier load can be calculated based on former analysis. The value of Z_L contains real part Z_{LR} and imaginary part X_{LR}, as Fig. 10-Fig. 11 shows. LCC circuit parameters C_{21} and L_{21} heavily affect Z_L value.

According to the results, both real and imaginary part of Z_L is not constant, which is causing problems on designing parameters for impedance matching circuit. As for linear load, we can design impedance matching circuit independently, because the load impedance and target impedance are definite. However, the equivalent impedance of rectifier load is time-varying, so a novel method to design the impedance matching parameters is in evitable to be put forward.

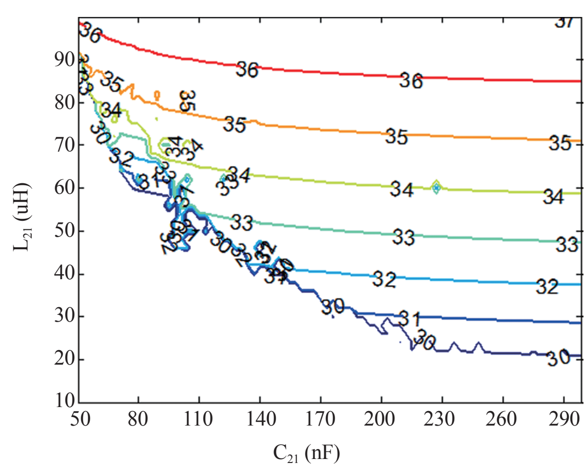

Fig. 10. The impedance impacts of L_{21} and C_{21} on R_{LR}, when R_L = 50 Ω.

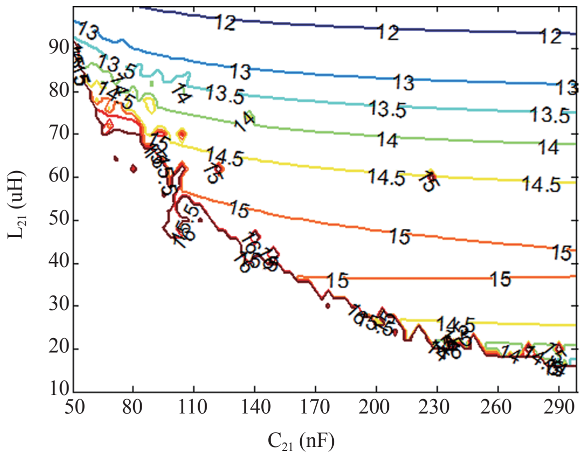

Fig. 11. The impedance impacts of L_{21} and C_{21} on X_{LR}, when R_L= 50 Ω.

Rectifier load only contains diodes, C_L and R_L, without inductance, but it is interesting that the equivalent impedance model of rectifier load can present *R*-*L* load.

IV. Design of LCC Parameters Under Rectifier Load

In order to meet the maximum efficiency condition, R_{21} is designed to equal R_{opt} by adjusting C_{21} and L_{21}, and secondary side circuit is tuned to resonant by C_S. According to the theory analysis, C_S is not necessary in some cases, and the impedance matching circuit can be translated into LCL topology.

When designing the LCC parameters L_{21}, C_{21} and C_S, there are many combinations satisfying the maximum efficiency condition. In order to choose one combination for WPT system, L_{21} or C_{21} can be determined firstly, and then compute others. According to the effect of L_{21} and C_{21} on R_{21}, as Fig. 12 shows, the value of C_{21} is more flexible to regulate R_{21}.

The variable β in (23) reflects the harmonic current in rectifier diodes, as Fig. 13 shows, which is even determined by L_{21} and C_{21}. When β becomes larger, the loss of diodes is obviously increasing because of the rectifier works from continuous

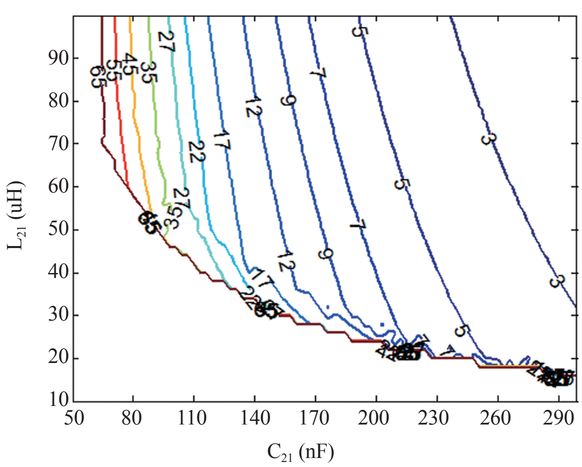

Fig. 12. The impedance impacts of L_{21} and C_{21} on R_{21}, when R_L= 50 Ω.

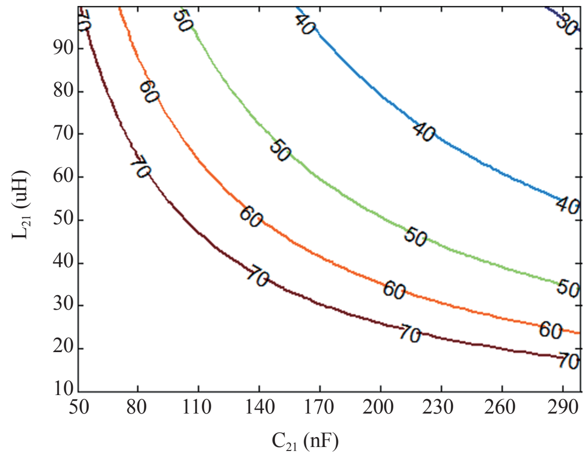

Fig. 13. The frequency impacts of L_{21} and C_{21} on high-frequency β (kHz), when R_L= 50 Ω.

conduction mode (CCM) to discontinuous conduction mode (DCM), meanwhile the peak current becomes larger, as Fig. 14 shows.

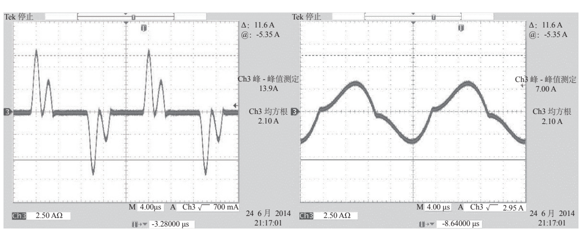

(a) Rectifier works in DCM (b) Rectifier works in CCM

Fig. 14. The current wave of rectifier diode using LCC impedance matching circuit. L_S= 165.7 uH, C_S= 117.3 nF, C_{21} = 161.9 nF, f=50 kHz.

It is obvious that we can increase L_{21} or C_{21} to decrease β value, and L_{21} is more suitable to enlarge the scope of impedance matching for rectifier load. Therefore, we can determine L_{21} firstly, and then compute C_{21} and C_S. L_{21} should be large enough to be optimized according to actual need, therefore, the initial value of L_{21} should be its maximum value, which can be determined according to experiences. When L_{21} is determined, we can analyze the effects of C_{21} on R_{21}, and decide its value according to $R_{21} = R_{opt}$. Then C_S can be tuned to resonant for secondary side circuit loop. If the conditions "$R_{21} = R_{opt}$" or "$Z_{21} = R_{opt}$" cannot be satisfied with the preset value of L_{21}, then its value should be decreased by 0.1μH in a loop until the conditions above are satisfied. A complete designing process of the secondary side LCC parameters is showed in Fig. 15.

After determining the value of the secondary side LCC network, the value of the primary side LCC network can be designed according to the conventional LCC compensation method [21]. It should be noticed that the value of "L", namely the inductance in the LCC network of the primary side, should be slightly larger(usually 10%~20%) than its theoretical value to guarantee an inductive load of the inverter, thus satisfying the ZVS condition of the system.

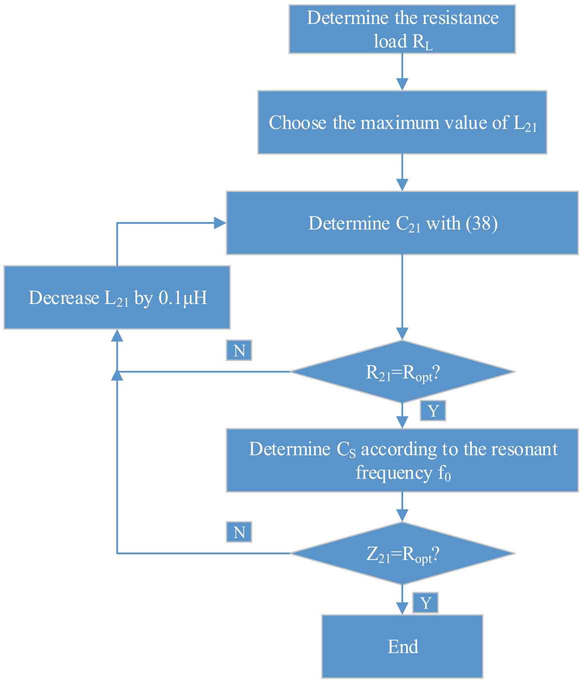

Fig. 15. Flowchart of the designing process of the LCC parameters.

V. Experimental Verification

Experiments are conducted to verify the design method of LCC impedance matching circuit under rectifier load. The WPT system is established as Fig. 16 shows, containing DC voltage source, voltage source inverter, primary coil and secondary coil, and dual-side LCC impedance matching circuits, rectifier circuit and load. The system parameters are shown in TABLE I.

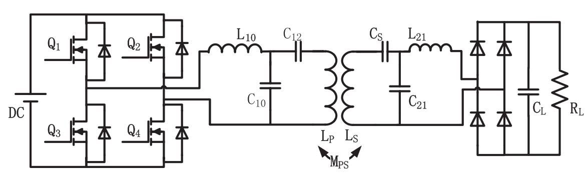

Fig. 16. WPT system circuit.

A. Impedance Matching for Different RL

According to WPT parameters in TABLE I, the optimal load for secondary coil and maximum efficiency can be theoretically calculated: R_{opt} = 9.6 Ω, and η_{max}= 97.35%. According to the proposed LCC impedance matching method, the rectifier load with different R_L can be matched by parameters in Fig. 17, where L_{21} = 86.1 uH. The transfer efficiency after LCC impedance matching is improved as Fig. 18 shows.

The transfer efficiency of the WPT system with the conventional C impedance matching(as Fig. 2 shows), the conventional LCC impedance matching [21] and the proposed LCC impedance matching is simulated separately. Due to the power losses of the converters and other components in the circuit, the efficiency does not reach the theoretical maximum efficiency η_{max}. However, it is obvious that compared to the conventional

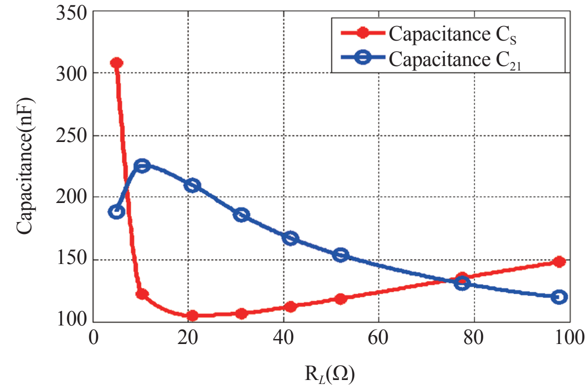

Fig. 17. The capacitors value and R_{21} at different actual load R_L conditions.

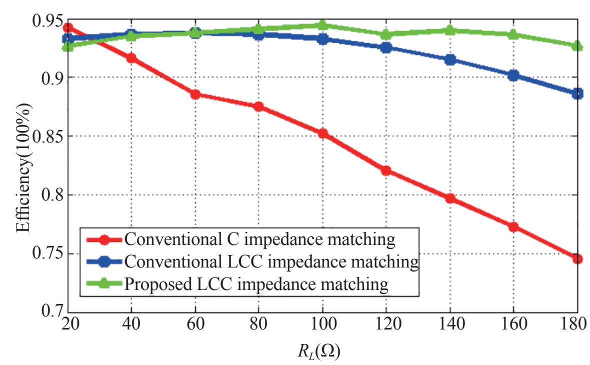

Fig. 18. The transmission efficiency η at different actual load R_L conditions.

impedance matching methods, the efficiency of the proposed impedance matching method is higher for different values of R_L, especially those far away from the optimum value.

B. 3.3 kW WPT System for EV Charging

The proposed LCC impedance matching method is applied to designing wireless charging system for electrical vehicle(EV), which can transfer 3.3 kW power over 20 cm distance. The coil subsystem of EV wireless charging system contains magnetic disk, coil layer and steel plate, as Fig. 19 shows. The steel plate is used to mimic the eddy current effect of EV chassis on coil. The magnetic disk adopts silicon steel sheet, which can not only decrease the eddy current loss, but also improve the quality factor and coupling coefficient.

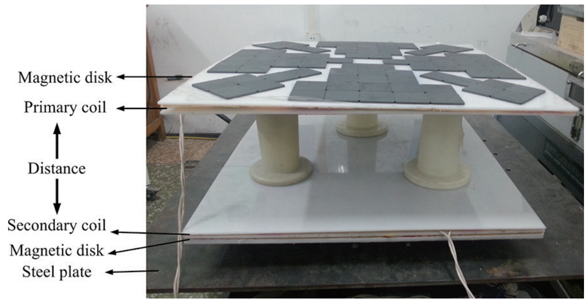

Fig. 19. Photo of wireless charging system.

Both primary and secondary coil is the same sizes, and wound by Litz line, as Fig. 20(a) shows.

(a) coil wounded by Litz (b) experiment result

Fig. 20. Coil and experiment result.

In our system, the battery is charging from 320 V to 350 V. When charging at the normal power, the charging voltage is 336 V, the charging current is about 9.8 A, and the equivalent R_L is about 34 Ω. Thus the secondary side parameters can be determined. Even more, primary side circuit parameters can be theoretically computed to meet the nominal power output after calculating the equivalent impedance of secondary side in TABLE II. WT1800 power analyzer is used to measure the system efficiency (end to end efficiency), as Fig. 20(b) shows, where Urm3, Irm3 and P3 are the input voltage, current and power, while Urm4, Irm4 and P4 are the output voltage, current and power, and η1 is the system efficiency. It can be seen that the system efficiency is about 92.7%.

TABLE II
Wireless Charging System Parameters

Parameter	Value	Parameter	Value
L_{10}	67.7 *uH*	L_{21}	86.1 *uH*
C_{10}	266.6 nF	C_s	112.75 nF
C_{12}	86.3 nF	C_{21}	175.7 nF
R_L	34 Ω	Coil Size	40 cm*40 cm

VI. Conclusion

This paper theoretically analyze the operation mechanical of secondary side LCC circuit under rectifier load, and then investigates the equivalent complex impedance calculation method for rectifier load, which is significant for theoretical designing to satisfy the maximum efficiency and normal power output. The proposed LCC impedance matching method can effectively improve transfer efficiency, especially when R_L is far away from optimum value. Typical WPT system researched in this paper, the optimum value of R_L is about 12 Ω, and the transfer efficiency gets the maximum value 97.2% without LCC impedance matching circuit. If $R_L \neq R_{opt}$, WPT system transfer efficiency with LCC impedance matching is obviously higher than the typical one. When $R_L > 30$ Ω, transfer efficiency with LCC is about 2% higher, and When $R_L > 60$ Ω, transfer efficiency with LCC is about 4% higher.

References

[1] J. C. Lin, "Wireless power transfer for cell phones or other mobile communication devices and biological implications," *IEEE Microwave Magazine,* vol. 14, no. 5, pp.18-22, 2013.

[2] H. Jiang, J. Zhang, and D. Lan *et al*., "A low-frequency versatile wireless power transfer technology for biomedical implants," *IEEE Transactions on Biomedical Circuits and Systems,* vol. 7, no. 4, pp. 526-535, 2013.

[3] S. Mohrehkesh and T. Nadeem, "Toward a wireless charging for battery electric vehicles at traffic intersections," in *2011 14th International IEEE Conference on Intelligent Transportation Systems (ITSC)*, 2011, pp.113-118.

[4] L. G. Xie, Y. Shi, and Y. T. Hou *et al*., "Wireless power transfer and applications to sensor networks," *IEEE Wireless Communications,* vol. 20, no. 4, pp.140-145, 2013.

[5] A. Kurs, A. Karalis, and R. Moffatt *et al*., "Wireless power transfer via strongly coupled magnetic resonances," *Science*, vol. 317, no. 5834, pp. 83-86, 2007.

[6] A. Karalis, J. D. Joannopoulos, and M. Soljačić, "Efficient wireless non-radiative midrange energy transfer," *Annals of Physics*, vol. 323, no. 1, pp. 34-48, 2008.

[7] B. L. Cannon, J. F. Hoburg, and D. D. Stancil *et al*., " Magnetic resonant coupling as a potentialmagnetic resonant coupling as a potential means forwireless power transfer to multiple small receivers," *IEEE Transactions on Power Electronics,* vol. 24, no. 7, pp. 1819-1825, 2009.

[8] M. Kiani and M. Ghovanloo, "The circuit theory behind coupled-mode magnetic resonance-based wireless power transmission," *IEEE Transactions on Circuits and Systems I: Regular Papers,* vol. 59, no. 9, pp. 2065-2074, 2012.

[9] S. H. Lee and R. D. Lorenz, "Development and validation of model for 95%-efficiency 220-W wireless power transfer over a 30-cm air gap," *IEEE Transactions on Industry Applications,* vol. 47, no. 6, pp. 2495-2504, 2011.

[10] T. Imura and Y. Hori, "Maximizing air gap and efficiency of magnetic resonant coupling for wireless power transfer using equivalent circuit and neumann formula," *IEEE Transactions on Industrial Electronics,* vol. 58, no. 10, pp. 4746-4752, 2011.

[11] T. C. Beh, T. Imura, and M. Kato *et al*., "Basic study of improving efficiency of wireless power transfer via magnetic resonance coupling based on impedance matching," in *IEEE International Symposium on Industrial Electronics (ISIE),* 2010, pp. 2011-2016.

[12] E. Bou, R. Sedwick, and E. Alarcon, "Maximizing efficiency through impedance matching from a circuit-centric model of non-radiative resonant wireless power transfer," in *2013 IEEE International Symposium on Circuits and Systems (ISCAS),* 2013, pp. 29-32.

[13] Y. Lim, H. Tang, and S. Lim *et al*., "An adaptive impedance-matching network based on a novel capacitor matrix for wireless power transfer," *IEEE Transactions on Power Electronics*, vol. 29, no. 8, pp. 4403-4413, 2014.

[14] Y. T. Luo, Y. M. Yang, and Z. S. Chen, " Network analysis and impedance matching methods for wireless power transfer via coupled magnetic resonances," *Industrial Design and Mechanics Power,* no. 437, pp. 301-305, 2013.

[15] Z. J. Zhang, N. W. Bergmann, and H. M. Li, "Analysis and design of LCCL load matching circuit for high-frequency induction heating series resonant inverter," *International Review of Electrical Engineering-IREE,* vol. 7, no. 5, pp. 5392-5399, 2012.

[16] Y. Zhang, Z. Zhao, and K. Chen, " Load matching analysis of magnetically-coupled resonant wireless power transfer," in *2013 IEEE Ecce Asia Downunder (Ecce Asia),* 2013, pp.788-792.

[17] J. Park, Y. Tak, and Y. Kim *et al*., "Investigation of adaptive matching methods for near-field wireless power transfer," *IEEE Transactions on Antennas and Propagation*, vol. 59, no. 5, pp. 1769-1773, 2011.

[18] K. Kusaka and J. Itoh, " Input impedance matched AC-DC converter in wireless power transfer for EV charger," in *2012 15th International Conference on Electrical Machines and Systems (ICEMS 2012),* 2012, pp. 1-6.

[19] C. Beh, M. Kato, and T. Imura *et al*., "Automated impedance matching system for robust wireless power transfer via magnetic resonance coupling," *IEEE Transactions on Industrial Electronics*, vol. 60, no. 9, pp. 3689-3698, 2013.

[20] K. E. Koh, T. C. Beh, and T. Imura *et al*., "Impedance matching and

power division using impedance inverter for wireless power transfer via magnetic resonant coupling," *IEEE Transactions on Industry Applications,* vol. 50, no. 3, pp. 2061-2070, 2014.

[21] S. Li, W. Li, and J. Deng *et al*., "A double-sided LCC compensation network and its tuning method for wireless power transfer," *IEEE Transactions on Vehicular Technology,* vol. 64, no. 6, pp. 2261-2273, 2015.

[22] J. Hou, Q. Chen, and S. C. Wong *et al*., "Analysis and control of series/series-parallel compensated resonant converter for contactless power transfer," *IEEE Journal of Emerging and Selected Topics in Power Electronics,* vol. 3, no. 1, pp. 124-136, 2015.

[23] H. Hao, G. A. Covic, and J. T. Boys, "An approximate dynamic model of LCL-T based inductive power transfer power supplies," *Power Electronics*, *IEEE Transactions on,* vol. 29, no. 10, pp. 5554-5567, 2014.

[24] J. Yin, D. Lin, and C. K. Lee *et al*., "A systematic approach for load monitoring and power control in wireless power transfer systems without any direct output measurement," *IEEE Transactions on Power Electronics,* vol. 30, no. 3, pp. 1657-1667, 2015.

[25] W. Zhang, S. C. Wong, and K. T. Chi *et al*., "Design for efficiency optimization and voltage controllability of series-series compensated inductive power transfer systems," *IEEE Transactions on Power Electronics,* vol. 29, no. 1, pp. 191-200, 2014.

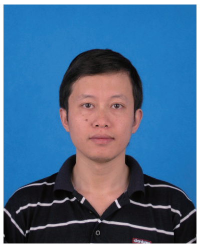

Chenglin Liao received the Ph.D. degree in Power Machinery and Engineering from Beijing Institute of Technology, Beijing, China, in 2001.

He is deputy director of Vehicle Energy System and Control Technology Division, Institute of Electrical Engineering Chinese Academy of Sciences. For the past 11 years at Institute of Electrical Engineering, He has been involved in research of battery manage system, vehicular control and wireless charging system for electric vehicle. Before coming to Institute of Electrical Engineering, he spent 2 years at Tsinghua University, where he was a postdoctoral researcher.

Junfeng Li received the Ph.D. degree at University of Chinese Academy of Sciences, Beijing, China, in 2015. He is now an engineer in Beijing Institute of Space Launch Technology. His research interests are wireless power tranfer and power electronics.

Shufan Li received his B.E. degree from Beijing Technology and Business University, Beijing, China, in 2013. Then he received his M.S. degree at University of Chinese Academy of Sciences, Beijing, China, in 2016, where he is currently working towards his Ph.D degree in Power Electronics and Electric Drive. His research interests includes: wireless power transfer theory, parameter estimation and control of wireless charging systems.